On the nature of dense CO adlayers

Cite as: J. Chem. Phys. **92**, 5034 (1990); https://doi.org/10.1063/1.458539
Submitted: 06 November 1989 . Accepted: 20 December 1989 . Published Online: 31 August 1998

B. N. J. Persson, M. Tüshaus, and A. M. Bradshaw

On the nature of dense CO adlayers

B. N. J. Persson
Institut für Festkörperforschung der Kernforschungsanlage Jülich, D-5170 Jülich, West Germany
M. Tüshaus and A. M. Bradshaw
Fritz-Haber-Institut der Max-Planck-Gesellschaft, Faradayweg 4-6, D-1000 Berlin 33, West Germany

(Received 6 November 1989; accepted 20 December 1989)

We have performed Monte Carlo simulations in order to study the ordered structures formed by CO on Pt{111} at high coverage. The results are compared with LEED and infrared (IR) spectra. The calculations are based on a recently constructed potential energy surface for CO on Pt{111} and a CO–CO interaction potential deduced from the variation of the CO binding energy with coverage. Ordered adsorbate structures are obtained at $\theta = 0.5$, 0.6, 0.67, and 0.71 in the simulations. The so-called compression structures ($\theta > 0.5$) are stabilized by the energy lowering which results when CO molecules at the high density domain walls move away from the on-top sites because of the unbalanced repulsive CO–CO interactions. If this relaxation channel is blocked, disordered adsorbate structures occur. We present the resulting (θ, T) phase diagram and discuss its qualitative properties. The LEED data show ordered structures at $\theta = 0.5$, 0.6, and 0.71, but, in contrast to previous results, or perhaps to the interpretation thereof, not at $\theta = 0.67$. The IR data show that the compression structures still consist of CO molecules adsorbed on distinct surface sites. Finally, we discuss the changes in adsorbate structures which would result from variations in the CO–substrate potential energy surface and, in the light of these results, briefly look at the Cu{111}–CO, Ni{111}–CO, and Pd{111}–CO chemisorption systems.

I. INTRODUCTION

Binding site determination in adsorbed layers is one of the central topics in surface science and enters directly into the discussion of many important processes at surfaces such as heterogeneous catalysis. The structure of ordered adsorbate systems is usually determined using low-energy electron diffraction (LEED). While this method gives directly the dimensions of the adsorbate unit cell it requires very involved calculations to determine binding sites and, if the unit cell contains more than one adatom or admolecule, the arrangement within the unit cell. In this paper we show how adsorbate structures can be obtained using Monte Carlo simulations[1] based on a potential energy surface constructed from infrared-reflection-absorption (IRAS) data on adsorbate vibrations,[2] and from information on the lateral interactions as deduced from the variation in the adsorbate binding energy with coverage. We focus mainly on dense adsorbate layers ($\theta > 0.5$), the so-called compression structures.

The nature of the compression structures formed by CO on the low index faces of Ni, Cu, Pd and Pt has been a subject of some discussion in the last twenty years. LEED investigations have shown that above $\theta = 0.5$ ordered arrays are formed which are more or less close-packed, but that the unit cells are not simply related to that of the substrate. As we shall see confirmed in this paper, the structure of such overlayers is due to a balance between the lateral repulsive interaction, which favors a hexagonal structure, and the adsorbate–substrate interaction, which tends to localize the molecules on specific, high symmetry sites. The structures themselves are, however, often very complex and it is only now that the details are beginning to emerge. At first it was believed that compression structures were due to strongly incommensurate, or "floating" phases, implying that the CO molecules are not bound to specific surface sites. However, the observation of C–O stretching frequencies characteristic of high symmetry sites (on-top, bridge, hollow) belies this assumption. It is now accepted that the CO compression structures are actually due to series of coincident site lattices.[3,4] These may be considered as consisting of phase and antiphase domains of some lower coverage structure ordered in a particular sequence. At the domain boundaries, or walls, there is a closer packing of the molecules in accordance with the higher coverage; adsorption on nearest neighbor sites may even occur. For the Pt{111}–CO system in the present investigation we show that the high-coverage structures are energetically stable only because the CO molecules at the antiphase boundaries can adjust to the repulsive CO–CO interaction by moving away from the on-top symmetry points. This motion costs relatively little energy owing to the low frequency of the parallel frustrated translation of the on-top bonded CO molecules. When this relaxation channel is blocked, disordered structures are obtained.

In the next section we discuss the Monte Carlo simulations for the Pt{111}–CO system as well as the adsorbate–substrate and CO–CO interaction potentials on which they are based. Section III briefly gives some experimental details. In Sec. IV the results of the Monte Carlo simulations are described and the temperature-coverage phase diagram derived. The LEED and IR data are reproduced in Sec. V and discussed in the context of the simulations. In the more general discussion of Sec. VI the dependence of adsorbate

 0021-9606/90/085034-13$03.00

structures on the details of the adsorbate–substrate potential is explored and the chemisorption systems Cu{111}–CO, Ni{111}–CO, and Pd{111}–CO are briefly considered.

II. THE MONTE CARLO SIMULATIONS

The necessary prerequisite for a Monte Carlo simulation of an adsorbate structure with more than one adsorption site is some knowledge of both the adsorbate–substrate potential energy surface and the lateral interaction potential. From IRAS[2,5,6] and electron energy loss spectroscopy[7] (EELS) it is known that for CO and Pt{111} only on-top and bridge sites are occupied at all adsorbate coverages and temperatures. Based on a detailed IRAS study of the temperature and coverage dependence of the internal C–O stretch vibration for this system, we have shown in an earlier paper,[2] how a semiempirical potential energy curve connecting the on-top and bridge sites can be constructed. The result is shown in Fig. 1. The CO binding energy is highest in the on-top site and about 60 meV smaller in the bridge site. The activation energy for CO diffusion is determined by the height of the barrier between the on-top and the bridge site and is about 0.3 eV according to Fig. 1. Note that the potential well at the on-top site is very flat: The local curvature corresponds to a frustrated translation frequency for CO of about $\omega_T \approx 49\ \mathrm{cm}^{-1}$. The local curvature at the bridge site is greater, corresponding to a frequency of $\omega_B \approx 300\ \mathrm{cm}^{-1}$. Both the activation barrier for diffusion and ω_T agree well with independent and more direct experimental measurements of these quantities.[8–10]

We now turn to the CO–CO interaction potential. For CO on Pt{111} both the static dipole–dipole and the van der Waals interactions are very weak and can be neglected. The dominant contribution comes from the indirect interaction via the substrate[11] and from the "Pauli repulsion" which results when two CO molecules are so close that the wave functions associated with their closed shells overlap. For CO on Pt{111} the CO–CO interaction potential is purely repulsive as can be deduced from the monotonic decrease in CO binding energy as a function of increasing coverage.[12,13] The CO–CO interaction potential is therefore taken as $U(r) = Ae^{-\alpha r} + A'e^{-\alpha' r}$ where A and $A' > 0$ and r is the CO–CO separation.[2] The first term in $U(r)$ represents the Pauli repulsion. For two CO molecules with their axes aligned parallel one can deduce from thermodynamic[14] and other data[15] that $A = 3.9\times10^4$ eV and $\alpha = 4.3\ \text{Å}^{-1}$. We have used these values for CO on Pt{111}. The second term in $U(r)$ arises from the more long-range ($\alpha' < \alpha$) interaction via the substrate. The parameters A' and α' have been determined such that (a) the CO binding energy decreases by the observed[13] 0.25 eV as the coverage increases from $\theta = 0$ to 0.5 and (b) the frequency of the frustrated translation increases from $\omega_T = 49$ to $60\ \mathrm{cm}^{-1}$ in the same coverage range as observed in inelastic helium scattering.[10] This gives $A' = 1.3$ eV and $\alpha' = 0.8\ \text{Å}^{-1}$. In Fig. 2(a) we show some important distances for CO on Pt{111} and in Fig. 2(b) the total potential $U(r)$ as well as the contribution from the indirect interaction alone.

The Monte Carlo simulations themselves have been per-

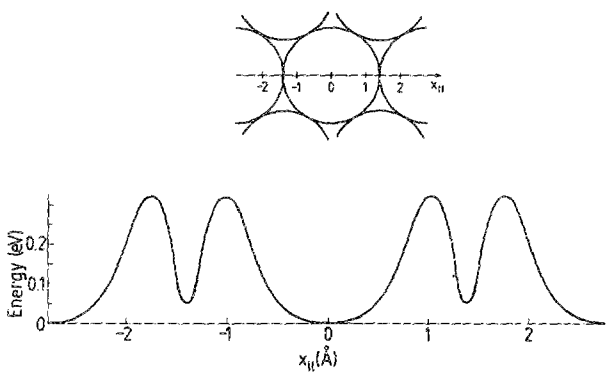

FIG. 1. Potential energy curve linking the on-top and bridge sites for CO on Pt{111}.

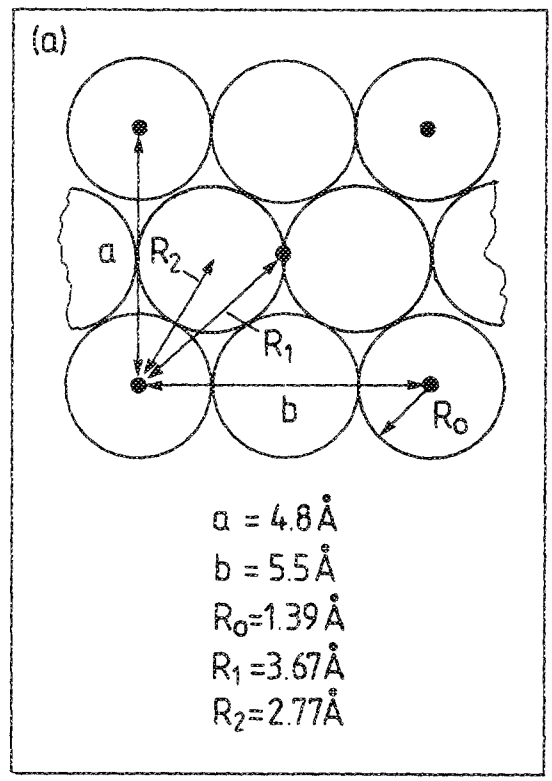

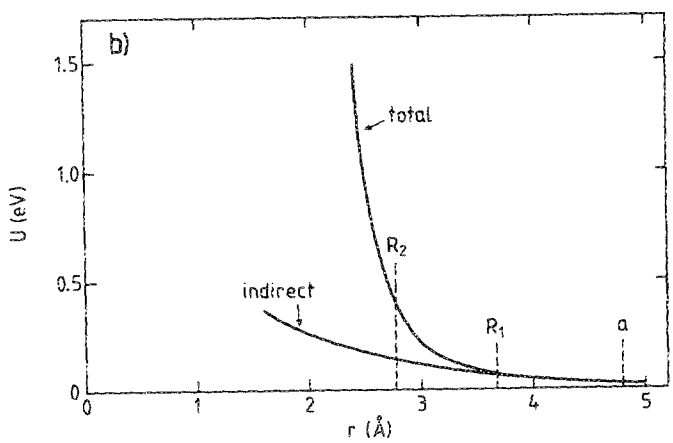

FIG. 2. (a) Intermolecular separations in the (4×2), or ($\sqrt{3}\times2$)rect, structure. (b) The lateral CO–CO interaction potential for CO on Pt{111}.

formed as follows. Although all the CO molecules occupy formally either on-top or bridge sites, they may be displaced slightly away from these symmetry sites by the unbalanced repulsive forces due to other CO molecules or simply due to the irregular thermal motion which occurs at nonzero temperatures. (The Monte Carlo simulations are based on classical statistical physics and therefore quantum mechanical effects such as zero point motion are not included). An on-top CO can jump to any of its six neighboring bridge sites, while a bridge CO can jump to one of its two neighboring on-top sites. In these jumps we allow for small random displacements away from the symmetry points. Futhermore, after each jump the CO molecules are allowed to readjust and thermalize in the wells. Any tentative change in the adsorbate positions is accepted or rejected according to the standard Monte Carlo prescription[16] so that after a long enough time the system will reach thermal equilibrium independent of the initial conditions. Figure 3 summarizes the procedure in detail: Consider a CO molecule at an on-top site but in general displaced from the high symmetry point. In the first step a random number r between zero and one is generated. If $r > p$, where p is an arbitrary but fixed number between zero and one (conveniently chosen so that the speed at which a nonequilibrium distribution relaxes to equilibrium is optimized), then the CO molecule is moved to a new position in the same on-top potential well. This change corresponds to vibrational motion in the potential well. Next, the coordinates (x, y) of the new position in the potential well are generated from two new random numbers r' and r'' $y = a(r'' - 0.5)$ where a is some conveniently chosen length of order of the diameter $2R$ of a metal atom. Next, the excitation energy ΔE associated with this move is calculated and another random number r''' is generated and if $r''' < e^{-\beta\Delta E}/(1 + e^{-\beta\Delta E})$ then the move is accepted. However, if this

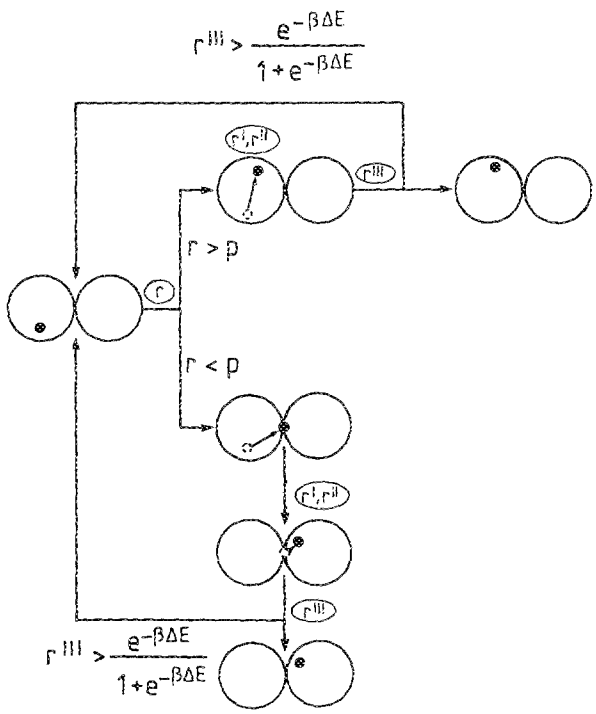

FIG. 3. A summary of the steps involved in the Monte Carlo calculations.

inequality is not satisfied the move is rejected and the old position is taken as the new coordinates. If $r < p$, the CO molecule is moved to a bridge site. This corresponds to a CO molecule jumping over the barrier between an on-top and a bridge site. Next, two new random numbers r' and r'' are generated in order to define the adsorbate position relative to the bridge site. The excitation energy ΔE is again calculated and the same condition as above is used to accept or reject the tentative move. The steps outlined above are repeated many times for all the CO molecules. After a sufficient number of these MC steps this prescription takes the system to thermal equilibrium as is easy to show by noting that the condition of detailed balance is satisfied.

All calculations have been made using periodic boundary conditions with the basic unit containing $M \times M$ Pt atoms, where M has been varied (typically $M = 8$, 10, 12, or 14). The CO molecules are placed initially in on-top positions on one side of the basic unit as shown in Fig. 4. The number N of CO molecules in the basic unit determines the CO coverage via $\theta = N/M^2$. Figure 4 shows, as an example, the result of a Monte Carlo calculation with 32 CO molecules on a 8×8 unit, i.e., at $\theta = 0.5$ and at the temperature $T = 250$ K. After 20 MC steps per particle only one CO molecule has changed sites. After 1000 MC steps per particle about half of the CO molecules have jumped (diffused) away from their original sites and after 100 000 MC steps per particle an almost perfect $c(4 \times 2)$ structure is obtained as observed experimentally. In addition to the vibrational excitations which give rise to small random displacements of the CO molecules away from the substrate symmetry points, one nonvibrational excitation occurs (denoted by T* in the figure). Here a bridge CO has jumped over the barrier between bridge and on-top sites, but because of the repulsive forces from the other nearby on-top CO molecules, it remains displaced in an elevated minimum about 0.4 Å away from the on-top site. This is the lowest energy nonvibrational excitation and is very important for the room temperature properties of the adsorption system.[2,17]

III. EXPERIMENTAL

A detailed description of the experimental apparatus has already been given in Ref. 2, so that only a brief summary of the essential features is given here. The system consists of a Fourier infrared spectrometer (Mattson, Sirius 100) housed in a large vacuum tank and coupled to the UHV chamber via KBr windows. An approximately $f/5$ cone of infrared radiation is reflected from the crystal at an average angle of incidence of 82° and refocused onto a narrow-band MCT detector. Spectra were usually recorded at 2 cm^{-1} resolution.

The UHV chamber is equipped with rear-view LEED optics, a quadrupole mass spectrometer, and facilities for argon ion sputtering. The Pt{111} crystal was cleaned by cycles of 500 eV argon ion bombardment followed by annealing at 900 K. It was mounted on a cold finger which allowed temperatures between 100 and 1500 K to be maintained.

The experimental spectrum in the C–O stretching region for the system Pt{111}–CO at $\theta = 0.5$ is shown in Fig. 5

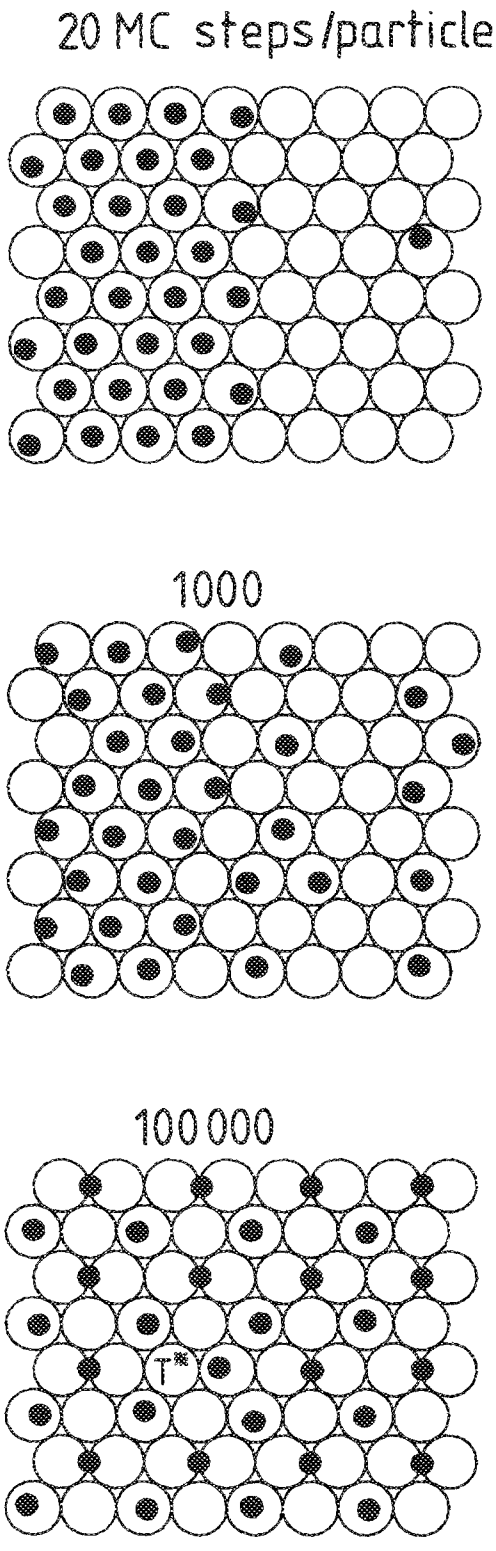

FIG. 4. The results of a Monte Carlo calculation at $T = 250$ K.

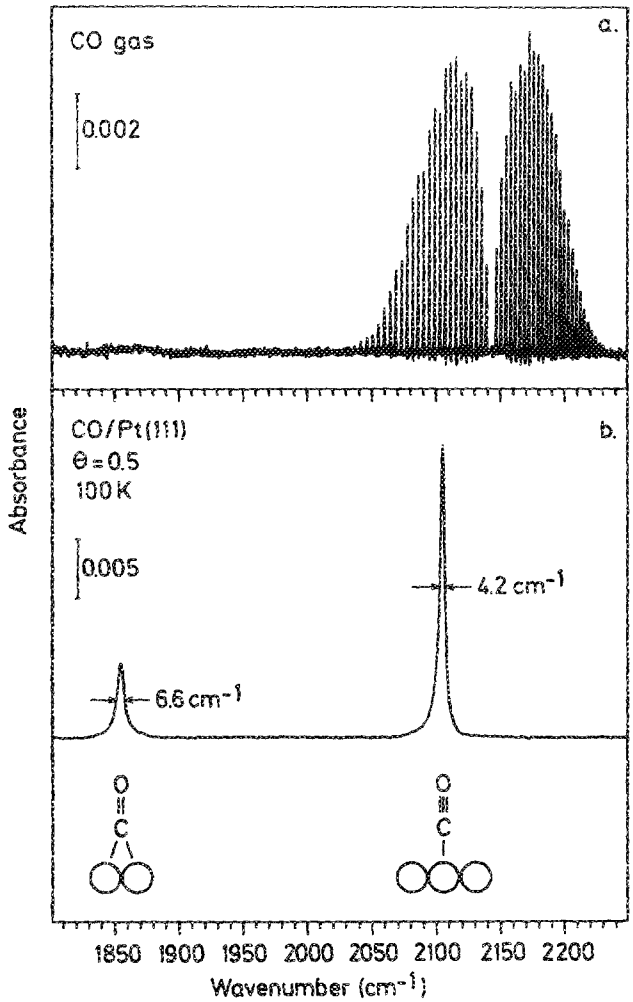

FIG. 5. (a) IR absorption spectrum of CO gas in the C–O stretching region, showing the rotational fine structure. (b) IRAS spectrum for CO on Pt{111} at $\theta = 0.5$ showing that the $c(4\times2)$, or $(\sqrt{3}\times2)$rect, structure consists of CO adsorbed on two discrete high symmetry sites: on-top and bridge.

(bottom). At this coverage a $c(4\times2)$ structure [designated $(\sqrt{3}\times2)$rect in the nonmenclature proposed by Biberian and Van Hove[3]] is formed consisting of equal numbers of on-top and bridge species.[18] This figure immediately illustrates the site specificity of the C–O strech and how it can be used in the characterization of adsorbed CO layers. At the same time it also illustrates one or two general features about infrared reflection–absorption spectroscopy (IRAS). Upon adsorption of a molecule on a surface the translational and rotational degrees of freedom are converted into vibrational degrees of freedom. Thus, the rotational fine structure present in the spectrum of the free molecule (Fig. 5, top) will disappear. In addition, the frequency, linewidth and intensity of the internal mode (as opposed to the external modes, the "frustrated" rotations and translations) will be affected by the interaction with the substrate. The considerable increase in linewidth, for example, is due to the new channels for nonradiative decay which open up in the adsorbed state (e.g., Ref. 2).

IV. THE ORDERED STRUCTURES AND THE PREDICTED PHASE DIAGRAM

Figure 6 shows the calculated variation in the relative CO bridge coverage N_B/N as a function of the coverage θ. The circles are the Monte Carlo results at 50 K obtained by cooling the system very slowly (typically 300 000 MC steps per particle) from $T = 500$ K. At low coverage only on-top sites are occupied which is easy to understand since this site has the largest binding energy and the temperature is not

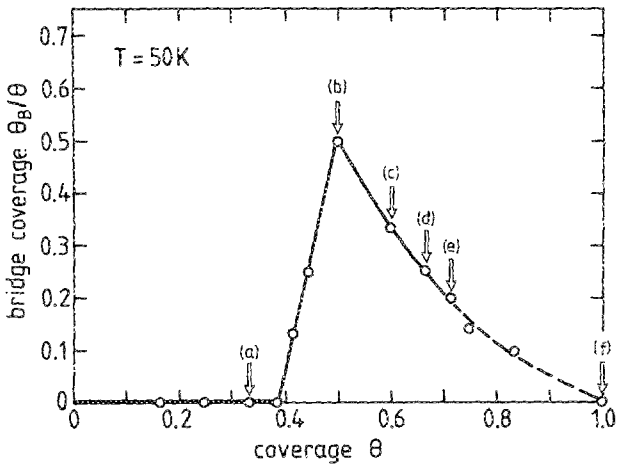

FIG. 6. The relative coverage of bridge CO as a function of total coverage. The arrows indicate the coverages where ordered structures are observed. The circles represent the Monte Carlo results obtained by slowly cooling from $T = 500$ to 50 K in about 300 000 MC steps per particle.

high enough to thermally populate the bridge sites. As the coverage increases above $\theta = 0.33$, the bridge site starts to become occupied. This results from the repulsive CO–CO interaction which tends to spread out the CO molecules as uniformly as possible on the surface. At $\theta = 0.5$ half of the CO molecules occupy the bridge sites. As θ increases beyond 0.5, the relative bridge coverage decreases so that finally at $\theta = 1$ all the on-top sites are occupied with zero bridge site occupation. The arrows in Fig. 6 indicate those coverages where ordered CO structures are obtained; Fig. 7 shows the resulting ordered patterns at $\theta = 0.5$, 0.6, 0.67, and 0.71. As we discuss in Sec. V below, these results are in good agreement with the LEED data, although there are some differences in the details. Note that $\theta = 1$ cannot be reached experimentally before the CO molecules start to desorb. We must at this point, however, make the following reservation. In the simulations of the ordered structures (see Fig. 7) we have used relatively small basic units ($M = 10$, 12 and 14). If other ordered structures were to exist which do not "fit" within the basic unit (i.e., are incompatible with the periodic boundary conditions) then these structures would not be obtained in the simulation. An example of this is provided by the (4×4) and (8×8) structures observed experimentally below $\theta = 0.5$. The simulations predict a $(\sqrt{3}\times\sqrt{3})R30°$ structure at $\theta = 0.33$ which in practice is not observed. The (4×4) and (8×8) structures, however, are based on small units of the $\sqrt{3}$ structure.[6] With a larger $M\times M$ basic unit it might be possible to reproduce these structures, although it is not clear whether the CO–CO interaction potential used here describes the long-range interaction well enough.

The structures above $\theta = 0.5$ in Fig. 7 consist of vertical strips of the $c(4\times2)$ structure [or $(\sqrt{3}\times2)$rect structure in the notation of Biberian and Van Hove[3]] forming a phase/antiphase sequence. They are separated by "fault lines," or domain walls, containing a higher density of CO molecules at on-top sites. Because of the unbalanced repulsive intermolecular interactions, the COs are shifted off the high-symmetry on-top sites by ~0.4 Å. The CO molecules in the Monte Carlo calculations are regarded as points. If such a displaced

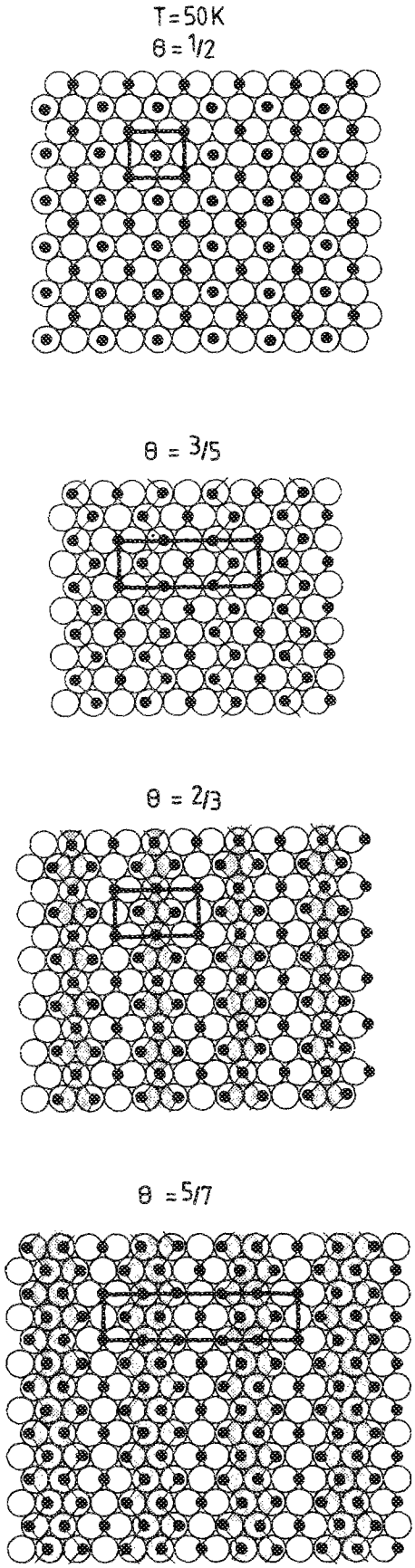

FIG. 7. The ordered structures at $\theta = 0.5$, 0.6, 0.67 and 0.71 for $T = 50$ K obtained from the Monte Carlo calculations. In the "rectangular" notation of Biberian and Van Hove (Ref. 3) these are designated $(\sqrt{3}\times2)$rect, $c(\sqrt{3}\times5)$rect, $(\sqrt{3}\times3)$rect, and $c(\sqrt{3}\times7)$rect, respectively. The unit meshes are shown accordingly.

point were to correspond to the center of mass of the molecule and its separation from the metal atom were to remain constant, the 0.4 Å displacement would imply a tilted C–O bond axis of $\sim 10°$, assuming that the C–O bond axis points to the center of the metal atom. That a 0.4 Å displacement from an on-top site gives rise to a tilt angle of $\sim 10°$ is substantiated by cluster calculations.[19] Note that the domain walls are different in each case: a single zigzag structure followed by two types of double zigzag.

The parallel CO displacements along the antiphase boundaries lower the total energy and, as we shall now show, without this relaxation none of the "compression" structures of Fig. 7 would be energetically stable. Figure 8 shows the result of a lattice gas Monte Carlo simulation at the coverage $\theta = 0.6$. This calculation is based on exactly the same model as above, but without allowing the CO molecules to move away from the high symmetry sites. In this case the resulting array is clearly disordered and the average energy per particle is now 37% higher than for the corresponding ordered structure shown in Fig. 7. Note that the relative low cost in energy required for the lateral displacement is due to the very flat potential energy surface at the on-top sites (see Fig. 1), i.e., to the low frequency of the frustrated translation for on-top CO. For the $\theta = 0.6$, 0.67, and 0.71 structures shown in Fig. 7 the relative bridge coverage N_B/N is 0.33, 0.25 and 0.20, respectively, while in the lattice gas simulation we find 0.62, 0.50, and 0.39, respectively. The higher occupation of the bridge sites in the lattice gas model is, of course, a consequence of the fact that occupying the on-top sites is energetically less favorable in this case. The average energy per adsorbed molecule both for the lattice gas model (parentheses) and for the full calculation where the molecules can move away from the high symmetry sites is given by: 360 (492), 470 (644), and 561 (780) meV for the $\theta = 0.6$, 0.67, and 0.71 structures, respectively. Here the energy zero is taken to correspond to a single CO molecule bonded in the on-top position. (The value at $\theta = 0.5$ is 250 meV, corresponding to the decrease in adsorption energy. This was an input parameter for the construction of the interaction potential in Sec. II above. The value is, of course, identical for both the lattice model and the full calculation.)

The schematic (θ, T) phase diagram for the Pt{111}–CO system resulting from the simulations is shown in Fig. 9. Here we only discuss the high-coverage region, $\theta > 0.5$. The areas denoted by I, II, and III indicate those regions where the $\theta = 0.6$, 0.67, and 0.71 structures shown in Fig. 7 are stable. The exact location of the phase boundaries is not known but this is of no direct relevance for what follows. At nonzero temperature (but below the melting temperature) and/or for small deviations away from the coverages 0.6, 0.67, and 0.71 the system is not "perfect" but has various types of imperfections; however, the long range order is the same as for the perfect I, II and III structures. At high enough temperature all the ordered structures "melt" into a fluid phase where no long-range order exists and where all on-top sites are occupied with equal probability. Similarly, all bridge sites are occupied with an equal probability which, however, differs in general from the on-top probability.

The shaded areas in Fig. 9 denote regions of incommensurate (IC) structure. The IC structure between the $c(4\times2)$, or $(\sqrt{3}\times2)$rect, structure and the phase I (coverage range $0.5 < \theta < 0.6$) consists of vertical strips of the $c(4\times2)$ structure separated by domain walls of the type already shown in Fig. 7 for the $\theta = 0.6$ structure. For $T > 0$ the walls will not be straight and equally spaced but will have kinks or more complex structure as indicated schematically in Fig. 10(a). We note here that the wall–wall interaction energy is extremely small when the separation between the walls is $n > 1$, where $n = 1,2,...$ is the number of $c(4\times2)$ strips between the walls. For $n = 1$ the interaction energy is about 12 meV per $(\sqrt{3}\times2)$rect unit. At a critical temperature (which depends on the adsorbate coverage) the IC structure melts. It has been shown that this melting transition occurs at the temperature where "dislocations" can be created spontaneously in the overlayer (dislocation unbinding).[20]

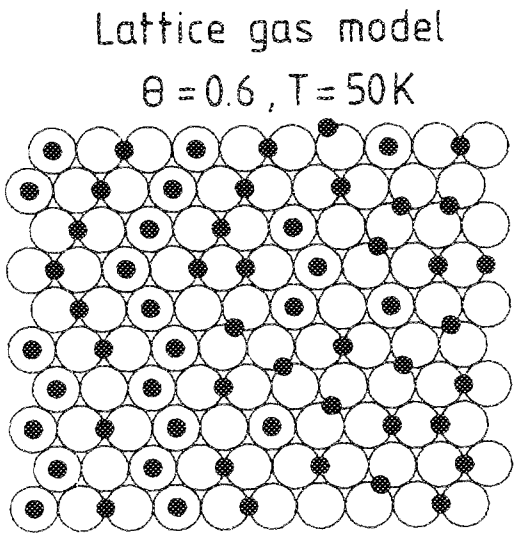

FIG. 8. Monte Carlo simulation ($\theta = 0.6$ and $T = 50$ K) based on the lattice gas model where the CO molecules are only allowed to occupy high symmetry sites.

Let us now instead keep the temperature fixed ($T < T_c$) and vary the coverage. Figure 10(b) shows a sequence of states expected as the coverage increases from 0.5 to 0.6. Since the commensurate (C) $c(4\times2)$ structure has the periodicity 2 in the x direction (the direction orthogonal to the walls in the IC phase), a direct C→IC phase transition cannot occur[21]: The $c(4\times2)$ and the IC phases must be separated by a fluid phase which exists down to zero temperature as indicated in Fig. 9. The melting of the $c(4\times2)$ structure with increasing θ is associated with dislocation unbinding as indicated in Fig. 10(b) and the phase transition is described by the Kosterlitz and Thouless theory of melting of two-dimensional harmonic solids. This theory can be applied in the present case because the system of domain walls constitutes effectively a two-dimensional (anisotropic) elastic solid: The elastic properties in the x direction are determined by the elastic forces between the walls caused by the loss of meandering entropy due to the collisions between walls and the elastic properties in the y direction arise from the bending energy of the walls. As the wall concentration increases the interaction between the domain walls will stiffen the elastic constants and resolidify the fluid phase.

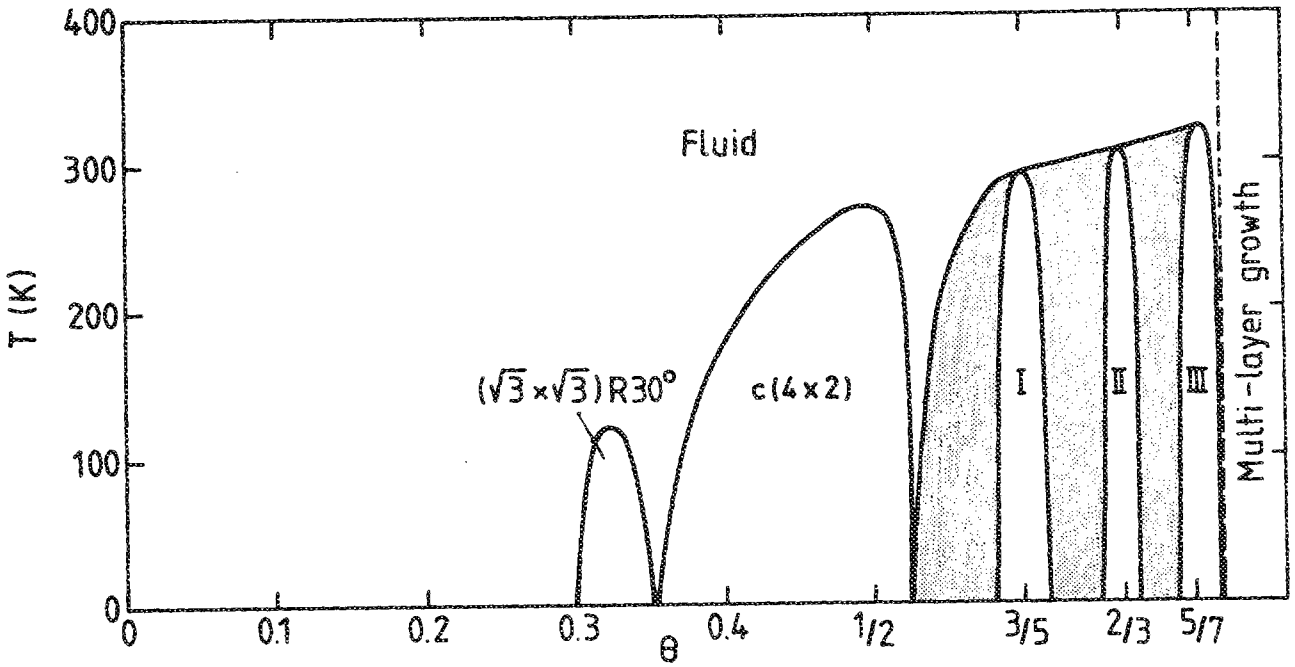

FIG. 9. Temperature-coverage phase diagram for the Pt{111}–CO chemisorption system. The shaded areas denote incommensurate phases while I, II and III denote the ordered phases shown in Fig. 7. The phase boundaries are not exactly known.

The IC regions between phases I and II as well as between phases II and III are of a different nature than that between the $c(4\times2)$ structure and phase I. In Fig. 10(c) we show the sequence of states expected as the coverage increases from 0.6 to 0.67. In the IC phase close to structure I a low concentration of domain walls characteristic of phase II (thick lines) in an otherwise perfect type I structure are expected. Due to the weak interaction between the domain walls they will be almost randomly distributed in the x direction, except at very low temperature. For $T>0$, the domain walls are not of infinite length, but consist of finite segments. This "breaking up" of the domain walls costs internal energy but is compensated by the increase in entropy. The same qualitative picture should hold in the incommensurate regions between phases II and III. This is illustrated by Fig. 11

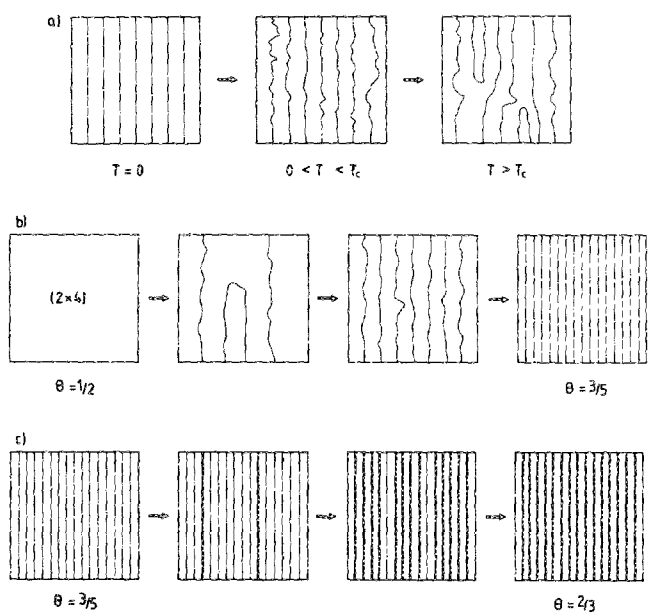

FIG. 10. (a) A schematic picture of the incommensurate structure occurring between the $c(4\times2)$ structure and phase I. The white areas denote strips of the $c(4\times2)$ structure and the thin lines the single zigzag domain walls. The melting temperature is denoted by T_c. (b) When the coverage increases from $\theta=1/2$ to 3/5, the adsorbate system first melts and then resolidifies (see the text for details). (c) Behavior of the system as the coverage increases from $\theta=3/5$ to 2/3. The thin and thick lines denote single zigzag and double zigzag domain walls, respectively. As before, the regions between are vertical strips of the $c(4\times2)$ structure.

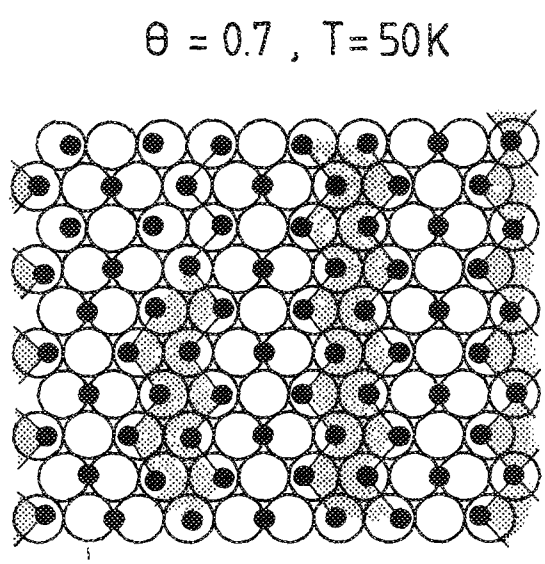

FIG. 11. The result of a Monte Carlo calculation at the coverage $\theta=0.7$ lying between phases II and III. Domain walls of both double zigzag types occur. Note the lattice imperfections which occur on the left-hand side resulting from the relatively fast cooling rate (200 000 MC steps per particle from $T=500$ to 50 K).

which shows the result of an MC calculation at $\theta = 0.7$ exhibiting domain walls characteristic of both phase II and phase III. Because of the relatively fast cooling rate in the MC simulation the structure has imperfections.

V. EXPERIMENTAL RESULTS

A. LEED

The sequence of LEED patterns observed for the system Pt{111}–CO for $\theta \geqslant 0.5$ is shown in Fig. 12. At $\theta = 0.5$ the well-known $c(4\times2)$, or $(\sqrt{3}\times2)$rect, structure is formed. Note that in common with all other structures on the surface there are three equivalent rotational domains. Increasing the CO coverage causes the extra features of the $c(4\times2)$ structure to become blurred and streaked. A typical diffraction picture between $\theta = 0.5$ and 0.6 is shown in Fig. 12(b). A careful examination of such pictures reveals that whereas three of the spots in the characteristic triangle of six appear to move in position, the other three show strong streaking effects. Kinematic LEED simulations[22] (allowing for the three rotational domains) show that these pictures are compatible with a real space model containing "on-top" domain walls identical to those found in the MC simulations of the $\theta = 0.6$ structure above. For the LEED simulations the domain walls are separated by strips containing a constant number of $c(4\times2)$ units. This gives rise to structures such as $c(\sqrt{3}\times25)$rect, $c(\sqrt{3}\times21)$rect, $c(\sqrt{3}\times17)$rect, $(\sqrt{3}\times13)$rect, $c(\sqrt{3}\times9)$rect corresponding to $c(4\times2)$ strip widths of 6, 5, 4, 3 and 2, respectively. In practice, the mutual repulsion of the domain walls is very weak (Sec. IV) and so no "domain wall superlattices" are formed. (This is not the case incidentally for Pd{111}; see Sec. VI). We therefore only expect streaking in the LEED pattern: In particular, those diffraction features will streak which show strong splittings on going from the $c(4\times2)$ to the $\theta = 0.6$ structure. This is illustrated schematically in Fig. 13(a). In some diffraction pictures in this coverage range there is evidence for discrete spots at the (1/2, 2/3) positions, which might indicate the formation of the $c(\sqrt{3}\times9)$rect structure. The latter is the only structure in this series to produce these features.

The pattern at $\theta = 0.6$ is shown in Fig. 12(c) and is that which would correspond to the structure resulting from the simulation in Fig. 7. The structure is designated $c(\sqrt{3}\times5)$rect and was suggested already by Biberian and van Hove,[3] although they were not in a position to distinguish whether the domain walls consisted of on-top or bridging species. The structure suggested by Avery[23] is not substantiated by the MC simulations nor would the corresponding domain walls give the observed splittings between $\theta = 0.5$ and 0.6.[22] On further increasing the coverage

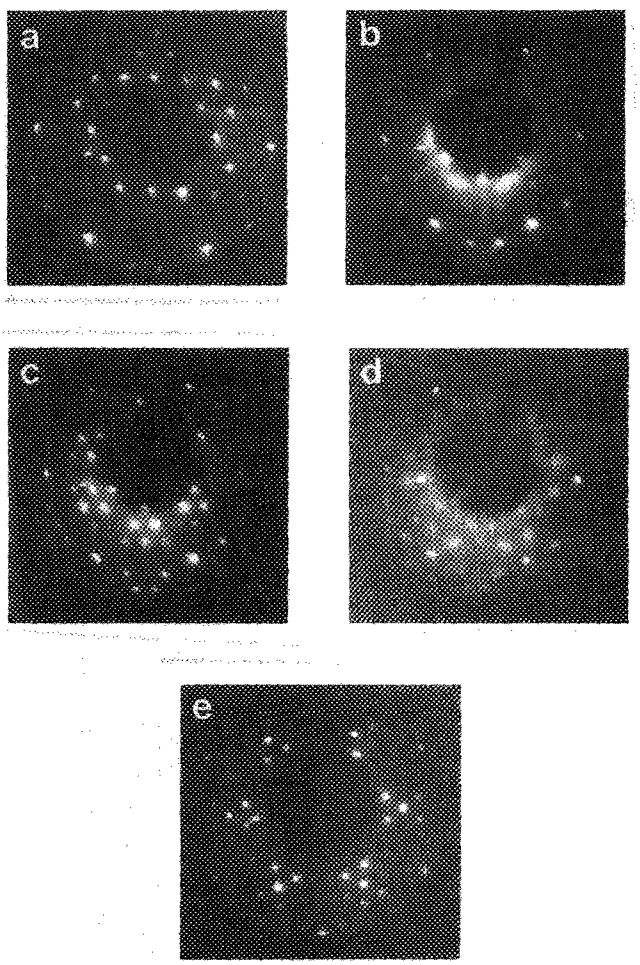

FIG. 12. Sequence of LEED patterns in the adsorption system Pt{111}–CO for $\theta \geqslant 0.5$. (a) $c(4\times2)$ at $\theta = 0.5$, 57 eV; (b) streaked $c(4\times2)$, 88 eV; (c) $c(\sqrt{3}\times5)$rect at $\theta = 0.6$, 88 eV; (d) streaked $c(\sqrt{3}\times5)$, 88 eV; (e) $c(\sqrt{3}\times7)$rect at $\theta = 0.71$, 119 eV.

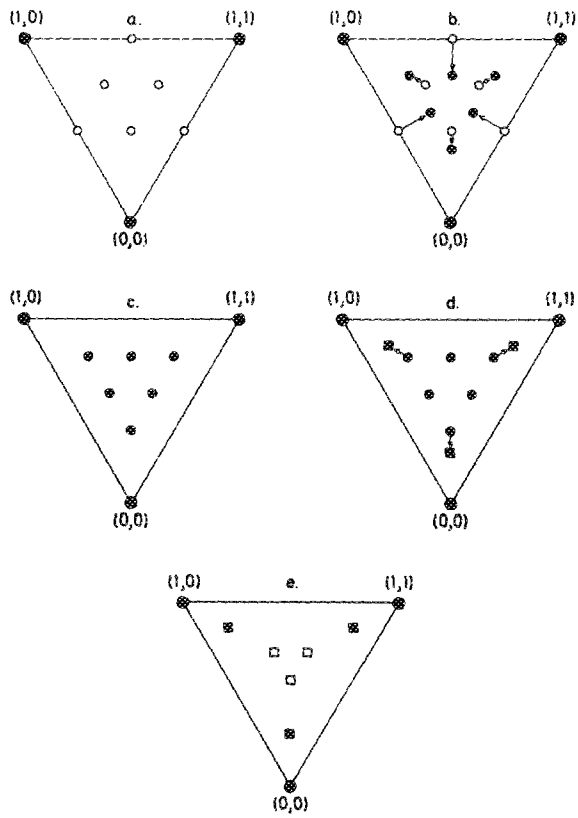

FIG. 13. Schematic representation of the LEED pattern sequence of Fig. 12 showing the transitions between the three ordered overlayers.

the next sharp LEED pattern [Fig. 12(c)] corresponds to the structure at $\theta = 0.71$ ($\theta = 5/7$) and may be designated $c(\sqrt{3}\times 7)$rect. The structure predicted by the MC simulations at $\theta = 0.67$ could not be observed in practice, although it is reported in the literature.[12,22,23] We are not sure whether earlier authors have mistaken the $c(\sqrt{3}\times 3)$rect at 0.71 for a $(\sqrt{3}\times 3)$rect at 0.67 or whether the $(\sqrt{3}\times 3)$rect structure occurs in such a narrow region of the (θ, T) phase diagram that we simple missed it. The fact that the MC simulations produce the structure suggests the latter but, on the other hand, we did carefully search for its diffraction pattern around $\theta = 0.67$. Avery[23] actually suggests the structure of Fig. 7 for an ordered overlayer at $\theta = 0.67$. The streaked intermediate structure [Fig. 12(d)] is characteristic of the coverages between $\theta = 0.6$ and 0.71. We have not performed any LEED simulations for this range, but the apparent movement of the extra diffraction features is indicated in Fig. 13(b).

B. Vibrational spectra

The IRAS data in the C–O stretching region corresponding to the sequence of LEED patterns of Fig. 12 are shown in Fig. 14. The first and most important conclusion to be drawn from the spectra is that the compression structures are indeed composed of on-top and bridging species, as indicated by the frequencies of the C–O stretches. Furthermore, these frequenceis are not too dissimilar from those in the $c(4\times 2)$ structure. There is, however, a somewhat surprising observation: Whereas a single sharp band at almost constant frequency is observed in the on-top region for $\theta \geqslant 0.5$, considerable structure is observed in the bridging region, particularly at the two coverages between the ordered overlayers. From the simulations of Fig. 7 one might expect that the $c(4\times 2)$, $c(\sqrt{3}\times 5)$rect and $c(\sqrt{3}\times 7)$rect structures would give rise in each case to a single *bridging* band. At first sight the results might therefore appear to support a model in which the domain walls are comprised of the bridging CO molecules. The diffraction patterns would be indistinguishable and, without the MC simulations, only the knowledge that the frustrated translation in the on-top site is of very low frequency would favor the structure models of Fig. 7. However, the bridge band/on-top band intensity ratio decreases by a factor 1.7 on going from the $c(4\times 2)$ to the $c(5\times\sqrt{3})$rect structure [and by 1.8 for the $c(7\times\sqrt{3})$rect structure]. Although IR intensities are not necessarily reliable guides to coverage at such high packing densities, it would be surprising if the corresponding changes in relative coverage in this case were actually in the reverse direction.

How can the apparent contradiction in the IR data be explained? An important factor is the phenomenon of dipole coupling (and the resulting intensity borrowing effects) which although possible to calculate with simple models at low coverage are difficult to quantify at high coverage. That the on-top band changes only by 2 cm^{-1} in frequency in going from $\theta = 0.5$ to $\theta = 0.71$ appears to be due to two mutually compensating effects. On one hand, the CO molecules are shifted off the on-top sites toward the bridge site at the domain wall which tends to *lower* their frequency. On the other hand, the increased local coverage of on-top (or "off-on-top") species increases the extent of dipole coupling which tends to *raise* the frequency. The shift of the bridging band from 1854 cm^{-1} at $\theta = 0.5$ to 1841 cm^{-1} at $\theta = 0.6$ may also result, at least in part, from dipole coupling. A glance at Fig. 7 shows that the separation between the bridging species increases, lowering the extent of dipole coupling and shifting the band to lower frequencies. The bands observed in between at 1848 and 1852 cm^{-1} may be due to intermediate structures unresolved in LEED. In any case the number of these species is probably much lower than suggested by the IR data on account of intensity borrowing. A conservative estimate would put their concentration at only a few per cent in the $c(\sqrt{3}\times 5)$rect spectrum. In the same way, the presence of the 1884 cm^{-1} band in the "streaked $c(\sqrt{3}\times 5)$rect" spectrum suggests that the concentration of the double zigzag domain walls is still quite low. The one inconsistency in the spectra of Fig. 14 lies in the position of the bridge band for the $c(\sqrt{3}\times 7)$rect structure: it is observed at a frequency of 1887 cm^{-1} [i.e., *higher* than that for the $c(4\times 2)$ structure], although the coverage of the bridging species is further reduced. We can only speculate that the origin of this effect is due to a direct or indirect chemical interaction between the bridging CO molecules and the on-top molecules along the antiphase boundary.

VI. DISCUSSION

A. General remarks

The results of the previous two sections enable us to conclude that the so-called compression structures in the

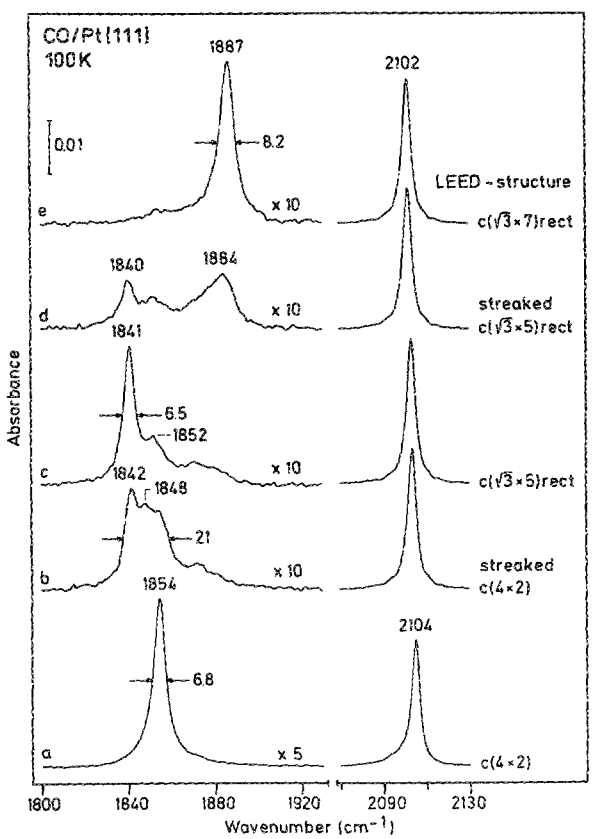

FIG. 14. Sequence of IRAS spectra taken parallel to the LEED data of Fig. 12.

adsorption system Pt{111}–CO are due to coincident site lattices and not to strongly incommensurate or floating phases. These coincident site lattices may be thought of as one unit strips of the $c(4\times2)$ structure (corresponding to $\theta=0.5$) separated by domain walls of higher CO density. In each case the domain walls consists of on-top CO: in the $c(\sqrt{3}\times5)$rect structure at $\theta=0.6$ it is a simple zigzag arrangement and in the $c(\sqrt{3}\times7)$rect structure at $\theta=0.71$ it is a double zigzag. The $(\sqrt{3}\times3)$rect structure predicted by the MC simulations at $\theta=0.67$, which was not observed in the present experiments, is characterized by a further type of domain wall (see Fig. 7). We return to this point briefly again below. These structures are only stable because CO molecules at the domain walls can lower the total energy by moving off the high symmetry on-top sites. The relatively small decrease in the CO–substrate binding energy associated with such displacements is related to the very low frequency for the parallel frustrated translation of on-top bonded CO. As discussed elsewhere, the low frequency of this mode also has other important consequences: (a) it is a strong driving force for phase transitions in the overlayer[17] (the large vibrational entropy associated with binding to the on-top sites tends to favor occupation of these sites at high temperature) and (b) the relative population of on-top and bridge sites at low adsorbate coverage is strongly influenced by the difference in vibrational entropy between the two sites.[2]

Confirmation of the conclusions drawn in this paper have come from recent ESDIAD studies of the Pt{111}–CO system by Kiskinova *et al.*[24] They measured the angular distribution of the CO^+ and CO* desorption products, which are due primarily to on-top CO. Consistent with the azimuthal orientation of the domain walls in the three rotational domains a hexagonal-like ESDIAD picture was obtained due to the tilted CO molecules. The C–O tilt angle was estimated to be $6°\pm1°$. Cluster calculations[19] have indicated that the ±0.4 Å displacement from the on-top site obtained in the MC simulations reported here would correspond to a tilting of the C–O axis by 10°. Another interesting result of Kiskinova *et al.* is the absence of untilted on-top CO (normally manifested by a central spot in the ESDIAD pattern) for the structures reported at $\theta=0.6$ and $\theta=0.67$. They noted the disagreement between Avery's structures[23] and the ESDIAD data. The correct structure at $\theta=0.6$ (see Fig. 7) has all the on-top CO in equivalent tilted configurations. We also suggest that the highest coverage structure investigated by Kiskinova *et al.* was the $c(\sqrt{3}\times7)$rect at 0.71 and not a $c(\sqrt{3}\times3)$rect at $\theta=0.67$ which would also bring their ESDIAD results into line with the structure models of Fig. 7.

We note that support for the notion of tilted CO species comes from the EELS data of Uvdal *et al.*[4] for the CO compression structures on Ni{100}, Cu{100}, and Pd{100}. They conclude that the frustrated rotations become dipole-allowed due to a bending of the M–C–O axis, which occurs in order that the CO–CO repulsion is reduced. (Note that a "bend" is not the same as a "tilt", but for present purposes the effect is the same.) This is, however, not the only mechanism, as the authors point out: When there is more than one CO molecule per unit cell, the forbidden "parallel" vibrations give rise to symmetric and antisymmetric combinations, the former being dipole-allowed. A very recent EELS paper by Voigtländer *et al.*[25] also indicates that a bent on-top adsorption site is occupied in the high-coverage $p2g(2\times1)$–CO structure on Ni{110}.

Finally, we point out that in the present calculations and also in Refs. 1 and 2 the platinum substrate has been assumed to be rigid. That this is a good approximation in the present context can be shown as follows. Consider two CO molecules bonded in the on-top position at two neighboring Pt atoms, e.g., at the domain wall in a compression structure. The strong, but short-range CO–CO interaction will tend to increase the mutual separation by displacing the CO molecules as indicated in Fig. 15(a) or by displacing the Pt atoms as indicated in Fig. 15(b). For a short wavelength Pt displacement as in Fig. 15(b) we can treat the metal atoms as Einstein oscillators characterized by the force constant $k_{\mathrm{Pt}}\approx M\omega_D^2$ where $M=196u$ is the mass of a Pt atom and $\omega_D\approx200\ \mathrm{cm}^{-1}$ the Debye frequency. The lateral variation of the CO–substrate binding potential at an on-top site determines the force constant $k\approx m\omega_T^2$, where $m=28u$ is the mass of the CO molecule and $\omega_T\approx49\ \mathrm{cm}^{-1}$ the resonance frequency for the parallel frustrated translation of on-top bonded CO. Hence $k/k_{\mathrm{Pt}}\approx0.01$, i.e., the substrate is very stiff and we can neglect the motion of the Pt atoms.

B. On the structure of fcc{111}–CO adlayers in general

The high coverage structures formed by CO on the surfaces of Ni, Cu, Pd, and Pt show certain general similarities, although of course many of the details are different. It is interesting to speculate as to how CO structures on fcc{111} surfaces depend in general on the difference E_T-E_B in the binding energy between the on-top and bridge sites. For this purpose we can perform similar calculations as above, taking the same CO–CO interaction potential and essentially the same CO–substrate potential, but allowing the relative well depths to vary. In this context we note that the chemisorption of CO on metal surfaces involves mainly the highest occupied 5σ orbital and the lowest unoccupied $2\pi^*$ orbital. The overlap between the substrate orbitals and the CO 5σ is greater at the on-top sites, less in the bridge sites and small in the three-fold hollow sites. Conversely, the overlap between the CO $2\pi^*$ and the substrate orbitals is largest in the three-fold hollow sites, less in the bridge sites and small in the on-top sites. Thus, if the substrate–5σ interaction is more important on-top sites would be occupied first and then, with

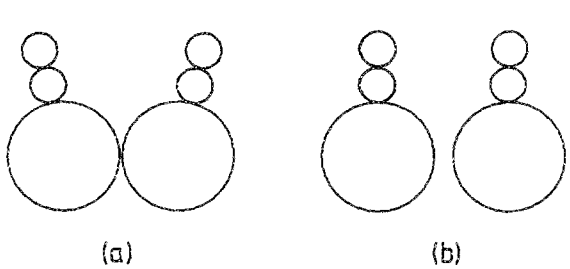

FIG. 15. The strong short-range repulsive CO–CO interaction could in theory result in (a) displaced and tilted CO molecules or (b) in displaced Pt atoms.

increasing coverage, bridge sites and finally threefold hollow sites. The first two stages of this bonding sequence occur for the Pt{111}–CO and Cu{111}–CO chemisorption systems. If instead the substrate–$2\pi^*$ interaction is more important one would expect to occupy the threefold hollow sites first and then, with increasing coverage, bridge sites and finally on-top sites. This bonding sequence is observed for the Ni{111}–CO and Pd{111}–CO chemisorption systems. There seems, however, to be no simple way of predicting theoretically if the 5σ–substrate or the $2\pi^*$–substrate interaction is the more important and in fact, since CO chemisorption on two such similar metals as Pd and Pt exhibits opposite sequences, this indicates that the explanation must lie in the finer details of the electronic structure.

Figures 16 and 17 summarize the results of the MC calculations for different value of $\Delta E = E_T - E_B$ obtained by slowly cooling from $T = 500$ K to $T = 50$ K. Figure 16(a) shows the variation of the relative bridge occupation $\theta_B/\theta = N_B/N$ where N is the total number of CO molecules and

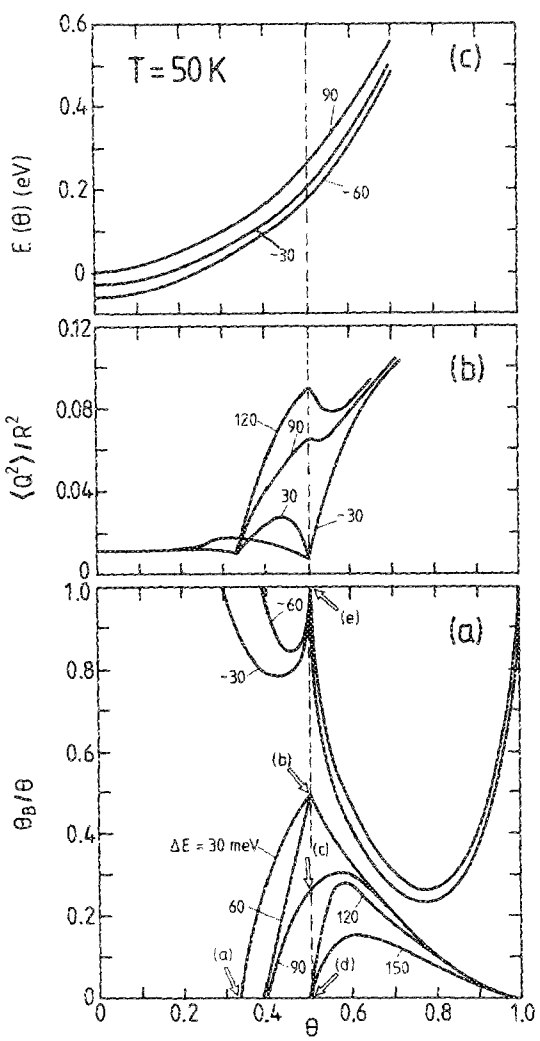

FIG. 16. (a) The relative bridge coverage θ_B/θ, (a) the mean square displacement $\langle Q^2 \rangle$ of the on-top CO molecules away from the on-top symmetry points and (c) the average energy per particle (with $E_T = 0$) as a function of the coverage θ. $\langle Q^2 \rangle$ is measured in units of R^2 where $R \approx 1.4$ Å is the radius of a Pt atom. The arrows in (a) indicate ordered structures. The results have been obtained by slowly cooling from $T = 500$ to 50 K.

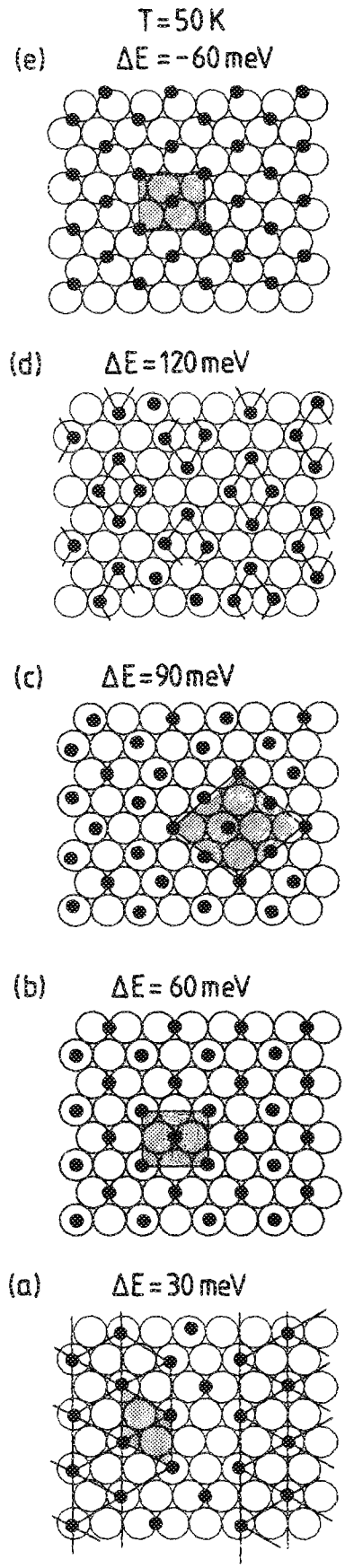

FIG. 17. The structures (a)–(e) denoted by arrows in Fig. 16(a). Note that the $(\sqrt{3}\times\sqrt{3})$R30° structure in (a) is imperfect because it is incompatible with the 8×8 basic unit. The $c(2\sqrt{3}\times4)$rect structure in (d) is also imperfect but in this case as a result of the too fast cooling rate in the MC calculation.

N_B the number of CO molecules in bridge sites. The arrows in this figure indicate ordered structures observed in the MC simulations. However, no systematic search for all the ordered structures was undertaken since this would have required using basic units of many different sizes and shapes. Most of the calculations were performed with an 8×8 unit for $E_T - E_B = \Delta E$ equal to -60, -30, 30, 60, 90, 120, and 150 meV. Four qualitatively different patterns of behavior can be distinguished:

(a) $0 < \Delta E < 75$ meV: The bridge coverage is zero up to $\theta = 0.33$. At this coverage the triangular adsorbate structure shown in Fig. 17(a) prevails. [The structure is not perfect since it is not compatible with the 8×8 basic unit; the actual coverage in Fig. 17(a) is $23/64 \approx 0.36$]. At $\theta = 0.5$ the usual $c(4\times2)$ structure occurs where half the CO molecules occupy the bridge site and the other half the on-top site [see Fig. 17(b)]. As expected, the coverage where bridge sites start to be occupied is shifted to higher θ as ΔE increases. Figure 16(b) shows $\langle Q^2\rangle$, the mean square displacement of the on-top CO molecules away from the on-top sites. This quantity is the sum of a contribution from the thermal motion which varies smoothly as a function of coverage plus a contribution from displacements of some on-top CO molecules away from the high symmetry points because of unbalanced forces from neighboring CO molecules. This latter contribution vanishes when the ordered structures are formed at $\theta = 0.33$ and $\theta = 0.5$, but gives rise to a "bump" between these two coverages as well as to the strong increase in $\langle Q^2\rangle$ for $\theta > 0.5$. For $\theta < 0.33$, $\langle Q^2\rangle$ is very small because of the short range of the CO–CO interaction compared to the CO–CO separations.

(b) 75 meV $< \Delta E <$ 105 meV: This is similar to case (a) but the ordered structure at $\theta = 0.5$ is different [see Fig. 17(c)] with a higher fraction of the molecules in on-top positions (75% instead of 50%). Note also that this structure has on-top molecules in displaced states as a result of unbalanced CO–CO interactions. This explains why $\langle Q^2\rangle$ is nonzero and large at $\theta = 0.5$ [see Fig. 16(b)].

(c) $\Delta E > 105$ meV: In this case no bridge sites are occupied for $\theta < 0.5$. At $\theta = 0.5$ the CO molecules form a $c(2\sqrt{3}\times4)$rect structure [see Fig. 17(d)] where all CO molecules occupy on-top positions. [The structure in Fig. 17(d) is not perfect as a result of too fast cooling]. Since the CO molecules experience unbalanced CO–CO interaction forces in this structure, they are all displaced away from the substrate symmetry points, giving rise to a local maximum in $\langle Q^2\rangle$ at $\theta = 0.5$ as seen in Fig. 16(b).

(d) $\Delta E < 0$: At low CO coverage only bridge sites are occupied. As a result of the CO–CO interaction, the on-top sites start to become occupied for $\Delta E = -30$ and -60 meV at $\theta \approx 0.3$ and $\theta \approx 0.4$, respectively. At $\theta = 0.5$ an ordered $c(4\times2)$ structure prevails with all the CO molecules in bridge sites as shown in Fig. 17(e). In this case $\langle Q^2\rangle$ is quite small until $\theta > 0.5$, where it increases quickly with increasing coverage just as the other cases studied above.

The energy per particle as a function of coverage is shown in Fig. 16(c). This quantity, in contrast to θ_B/θ and $\langle Q^2\rangle$, changes smoothly with increasing coverage. Note also that for $\theta > 0.6$, $\langle Q^2\rangle$ is very similar for all the cases studied; this simply reflects the strong repulsive interactions which occur in the compression structures and which now dominate over the energy difference ΔE between the on-top and bridge sites.

In discussing other experimental data in the light of the results presented above, we should first note that the CO–CO interaction potential used in the calculations was chosen to reproduce the gross properties of the CO–CO interaction on Pt{111}. Furthermore, the occupation of the three-fold hollow sites is not allowed in the calculations. There is thus no reason to expect our calculations to be able to describe in detail the properties of other CO chemisorption systems. With these reservations in mind, we briefly consider the Cu{111}–CO, Ni{111}–CO, and Pd{111}–CO systems where the lateral CO–CO interactions are also repulsive.

For CO on Cu(111)[26–28] the on-top sites have the largest binding energy and only these sites are occupied at low CO coverage. At $\theta = 0.33$ the sharp features of $(\sqrt{3}\times\sqrt{3})$R30° structure are observed as predicted by the model calculation above. The bridge sites start to be occupied first at $\theta \approx 0.44$, which [if the CO–CO interaction has a similar strength as in the Pt{111}–CO system] indicates an energy difference between the on-top and bridge sites of about 100 meV [see Fig. 16(a)]. In the coverage range $0.33 < \theta < 0.44$ there is some experimental evidence for tilted on-top CO molecules as the frustrated rotation of CO can be observed in the electron energy loss spectra (this mode is normally dipole forbidden). This again agrees well with the model calculations which show relatively large CO displacements away from the high symmetry sites in this coverage regime. Associated with these displacements is a tilting of the on-top CO molecules and as a result the frustrated rotation becomes dipole-allowed.

For CO on Ni{111}[29–31] the threefold hollow site has the largest binding energy. However, already for $\theta > 0.15$ all the CO molecules occupy bridge sites, since this can give rise to a more uniform adsorbate packing and to a lower total energy. Since the coverage at which the switch from threefold hollow to bridge occurs is very low, the energy difference between these sites must be very small. At $\theta \approx 0.3$ the on-top sites start to become occupied and θ_T/θ increases until θ is very close to 0.5 where the on-top occupation quickly drops to zero and a $c(4\times2)$ structure is formed with all CO molecules in bridge sites. This behavior agrees with the $\Delta E = -30$ meV curve in Fig. 16(a) and the structure of Fig. 17(e). The ordered structure at $\theta = 0.5$ shown in Fig. 17(e) agree with that proposed by Erley *et al.*[29] When θ increases beyond 0.5 the on-top sites becomes occupied again in agreement with the simulation result in Fig. 16(a).

For CO on Pd{111}[32] the threefold hollow site also has the deepest potential well. The $(\sqrt{3}\times\sqrt{3})$R30° structure formed at $\theta = 0.33$ is entirely composed of threefold hollow CO. At $\theta = 0.5$, however, only bridge sites are occupied giving the same $c(4\times2)$ structure as for Ni{111} [Fig. 17(e)]. However, the energy difference between threefold hollow and bridge is clearly somewhat greater than on Ni{111}. Up to $\theta = 0.6$ the domain walls of the compression structure are composed entirely of bridging CO and at higher coverages on-top sites are also occupied. Finally, at $\theta = 0.75$ the

(2×2) structure is composed of on-top and threefold hollow species. The Pt{111}–CO system is more difficult to compare with the model calculations, because of the involvement of the threefold hollow species over an extended coverage range. It does, however, show interesting parallels with Pt{111}–CO in the coverage range $0.33<\theta<0.6$ with respect to the domain wall structures.[32]

VII. SUMMARY

In this paper we have presented Monte Carlo simulations of the so-called compression structures in the Pt{111}–CO chemisorption system and compared them with LEED and IRAS data. The calculations are based on a potential energy surface constructed from a detailed IRAS study of the C–O stretch vibration, and on the lateral CO–CO interaction potential deduced from thermodynamic data for gas-phase and adsorbed CO. Ordered adsorbate structures were obtained at $\theta=0.6$, 0.67, and 0.71 in the simulations and consist of coincident site lattices based on the $c(4\times2)$ structure (obtained at $\theta=0.5$). In an equivalent description the structures may be considered as containing equally spaced domain walls of higher CO density, which separate strips of single $c(4\times2)$ units. Such structures are found to be energetically stable only because the on-top CO molecules at the domain walls can adjust to the repulsion CO–CO interaction energy by moving a few tenths of an Ångstrom off the on-top sites. We have presented a (θ, T) phase diagram based on the results of the simulations and discussed its qualitative properties. In practice, the LEED data show ordered structures at $\theta=0.6$ and 0.71 but not at 0.67. It is possible that previous authors have mistaken the $c(\sqrt{3}\times7)$rect structure at 0.71 for a $(\sqrt{3}\times3)$rect structure at 0.67. This is supported by recent ESDIAD data from the Yates group. The IR data confirm that the compression structures still consist of CO molecules adsorbed on distinct surface sites. The changes in the spectra as a function of coverage are consistent with the domain wall model. Finally, we have looked at the variation in the nature of the adsorbate structure as a function of the energy difference $\Delta E=E_T-E_B$ between the on-top and bridge binding sites, and discussed the Cu{111}–CO, Ni{111}–CO, and Pd{111}–CO systems in the light of these results.

ACKNOWLEDGMENTS

We would like to thank H. Conrad and W. Selke for many useful discussions. We acknowledge financial support from the Deutsche Forschungsgemeinschaft through Sonderforschungsbereich 6 and from the Fonds der Chemischen Industrie.

[1]B. N. J. Persson, Solid State Commun. **70**, 211 (1989).
[2]E. Schweizer, B. N. J. Persson, M. Tüshaus, D. Hoge, and A. M. Bradshaw, Surf. Sci. **213**, 49 (1989).
[3]J. P. Biberian and M. A. Van Hove, Surf. Sci. **118**, 443 (1982); **138**, 361 (1984).
[4]P. Uvdal, P.-A. Karlsson, C. Nyberg, S. Andersson, and N. Richardson, Surf. Sci. **202**, 167 (1988).
[5]R. G. Tobin and P. L. Richards, Surf. Sci. **179**, 387 (1987).
[6]M. Tüshaus, E. Schweizer, P. Hollins, and A. M. Bradshaw, J. Electron Spectrosc. **44**, 305 (1987), and references therein.
[7]H. Steininger, S. Lehwald, and H. Ibach, Surf. Sci. **123**, 264 (1982).
[8]B. Poelsema, L. K. Verheij, and G. Comsa, Phys. Rev. Lett. **49**, 1731 (1982).
[9]J. E. Reutt-Robey, D. J. Doren, Y. J. Chabal, and S. B. Christmann, Phys. Rev. Lett. **61**, 2778 (1988).
[10]A. M. Lahee, J. P. Toennies, and Ch. Wöll, Surf. Sci. **177**, 371 (1986).
[11]T. L. Einstein and J. R. Schrieffer, Phys. Rev. B **7**, 3629 (1973); T. B. Grimley, Proc. Phys. Soc. **90**, 751 (1967).
[12]G. Ertl, M. Neumann, and K. M. Streit, Surf. Sci. **64**, 393 (1977).
[13]E. G. Seebauer, A. C. F. Kong, and L. D. Schmidt **176**, 134 (1986).
[14]E. A. Mason and W. E. Rice, J. Chem. Phys. **22**, 843 (1954).
[15]T. Kihara and H. Koide, Adv. Chem. Phys. **33**, 52 (1975).
[16]See, for example, *Monte Carlo Methods in Statistical Physics*, edited by K. Binder (Springer, Berlin and Heidelberg, 1979).
[17]B. N. J. Persson, Solid State Commun. **70**, 215 (1989).
[18]D. F. Ogletree, M. A. Van Hove, and G. A. Somorjai, Surf. Sci. **173**, 351 (1986).
[19]B. N. J. Persson and J. E. Müller, Surf. Sci. **171**, 219 (1986).
[20]J. Villain, in *Ordering in Strongly Fluctuating Condensed Matter Systems*, edited by T. Riste (Plenum, New York, 1980).
[21]S. N. Coppersmith, D. S. Fisher, B. I. Halperin, P. A. Lee, and W. F. Brinkmann, Phys. Rev. Lett. **46**, 549 (1981).
[22]H. Conrad and A. M. Bradshaw (unpublished results). These simulations also exclude the possibility that the compression structures are strongly incommensurate, or floating, phases.
[23]N. Avery, J. Chem. Phys. **74**, 4202 (1981).
[24]M. Kiskinova, A. Szabo, and J. T. Yates, Jr., Surf. Sci. **205**, 215 (1988).
[25]B. Voigtländer, D. Bruckmann, S. Lehwald, and H. Ibach, Surf. Sci. **225**, 151 (1990).
[26]J. Pritchard, Surf. Sci. **79**, 231 (1979).
[27]B. Hayden, K. Kretschmar, and A. M. Bradshaw, Surf. Sci. **155**, 533 (1985).
[28]R. Raval, S. F. Parker, M. E. Pemble, P. Hollins, J. Pritchard, and M. A. Chesters, Surf. Sci. **203**, 353 (1988).
[29]W. Erley, H. Wagner, and H. Ibach, Surf. Sci. **80**, 612 (1979).
[30]L. Surnev, Z. Xu, and J. T. Yates, Surf. Sci. **201**, 1 (1988).
[31]J. G. Chen, W. Erley, and H. Ibach, Surf. Sci. **223**, L891 (1989).
[32]M. Tüshaus, W. Berndt, A. M. Bradshaw, and B. Persson, Appl. Phys. (in press).